Research Article | Vol. 27, No. 16 | 5 Aug 2019 | OPTICS EXPRESS 23396
Optics EXPRESS

Second-order coherence function of a plasmonic nanoantenna fed by a single-photon source

NIKITA E. NEFEDKIN,[1,2,3,*] EVGENY S. ANDRIANOV,[1,2] ALEXANDER A. ZYABLOVSKY,[1,2] ALEXANDER A. PUKHOV,[1,2,3] ALEXEY P. VINOGRADOV,[1,2,3] AND ALEXANDER A. LISYANSKY[4,5]

[1]*Dukhov Research Institute of Automatics, 127055 Moscow, Russia*
[2]*Moscow Institute of Physics and Technology, 141700 Moscow Region, Russia*
[3]*Institute for Theoretical and Applied Electromagnetics, 125412 Moscow, Russia*
[4]*Department of Physics, Queens College of the City University of New York, NY 11367, USA*
[5]*The Graduate Center of the City University of New York, NY 10016, USA*
**nefedkin@phystech.edu*

Abstract: We study the second-order coherence function of a plasmonic nanoantenna fed by near-field of a single-photon source incoherently pumped in the continuous wave regime. We consider the case of a strong Purcell effect, when the single-photon source radiates almost entirely in the mode of a nanoantenna. We show that when the energy of thermal fluctuations, kT, of the nanoantenna is much smaller than the interaction energy between the electromagnetic field of the nanoantenna mode and the single-photon source, $\hbar\Omega_R$, the statistics of the emission is close to that of thermal radiation. In the opposite limit, $\hbar\Omega_R >> kT$, the nanoantenna radiates single photons. In the last case, we demonstrate the possibility of overcoming the radiation intensity of an individual single-photon source. This result opens the possibility of creating a high-intensity single-photon source.

1. Introduction

Recently, the development of single-photon sources (SPSs) has grown considerably. The main application area for these sources is the encoding/decoding of quantum information [1,2], quantum computing [3], quantum cryptography [4], and manipulations of individual quantum objects, such as qubits [2,5]. For nano-photonic applications, single photons are produced by quantum dots [6,7], single molecules [8], atoms in cavities [9], and nitrogen-vacancy (NV) centers [10–12].

SPSs suitable for nanophotonic applications have an important drawback in that their radiation rate is low [13]. The characteristic radiation rate of SPSs based on solid-state quantum emitters does not exceed one radiation event per nanosecond. This radiation rate could be increased by placing an SPS inside an open resonator, i.e. using the Purcell effect [14]. This increase is proportional to the quality factor of the resonator and is inversely proportional to the volume of the resonator mode.

In nano-optics, a system consisting of an antenna and an SPS should be nanosized. Metallic plasmonic nanoantennas satisfy this requirement. In such a system, the role of the resonator mode is played by localized surface plasmons. Although the Q-factor of plasmonic structures is relatively low, due to the small volume of the modes, the Purcell factor reaches a value of $\sim 10^2 - 10^4$ [11,12,15,16]. Then, one could expect that an SPS can radiate at the rate of one photon per picoseconds, which is much higher than the rate of SPSs based on solid-state quantum emitters, e.g. quantum dots or NV centers.

#368192 https://doi.org/10.1364/OE.27.023396
Journal © 2019 Received 22 May 2019; accepted 27 Jul 2019; published 31 Jul 2019

Optics EXPRESS

For many applications, it is important to know how the antenna-SPS system radiates. Note that when the Purcell factor is large, the SPS mainly radiates in resonator mode [17,18]. In other words, an excited SPS passes the main part of the energy to a nanoantenna, which then reradiates this energy. Since the characteristic radiation rate of plasmonic structures is several orders of magnitude greater than the radiation rate of SPS, we achieve a desirable increase in intensity.

On the other hand, since a nanoantenna without an SPS is in thermal equilibrium, it radiates as a black body with a second-order coherence function $g^{(2)}(0)=2$ [19,20]. Thus, the system may no longer radiate single photons, even though $g^{(2)}(0)=0$ for an SPS. This has been confirmed by recent experimental results involving measurements of the radiation statistics of plasmonic structures interacting with SPSs [21–32]. In the overwhelming majority of these experiments, $g^{(2)}(0)$ of the radiation of an antenna-SPS system has a value of a few tenths. Some of these experiments even demonstrate super-Poisson statistics, with $g^{(2)}(0)>1$ [25,29,31]. However, if an SPS passes only one photon into the antenna mode, we can expect this photon to be radiated by the antenna before thermalization.

It has recently been theoretically shown that a plasmonic nanoantenna may produce single-photon radiation if it is excited by coherent pumping [33], or if coherent population trapping is used in a three-level system [34]. However, *incoherent* pumping is also widely used and more easily achieved in practical realizations of SPSs.

In this paper, we demonstrate that it is possible for an antenna-SPS system to emit single photons under *incoherent* pumping of the SPS. Using computer simulation, we show that for a plasmonic nanoantenna-SPS system, the values of the second-order coherence function, $g^{(2)}(0)$, are in the range from 0 to 2, depending on the ratio of the energy of thermal fluctuations, kT, of the nanoantenna and the interaction energy, $\hbar\Omega_R$, between the mode of the nanoantenna and the SPS. For $\hbar\Omega_R << kT$, the Purcell factor is small, as is the part of the energy transferred from the emitter to the antenna; as a result, the nanoantenna radiates as a black body with $g^{(2)}(0)=2$. For $\hbar\Omega_R >> kT$, the Purcell factor and the radiation rate are large. In such a case, the rearrangement of the quantum states of the nanoantenna effectively gives single-photon emission. In this case, $g^{(2)}(0)$ can reach zero. The obtained result can be used to create nanoscale ultrafast SPSs based on plasmonic nanoantennas.

2. The model

We consider a plasmonic nanoantenna, which size is much less than the radiating wavelength in a free space, fed by an SPS. We assume that the SPS is a two-level system (TLS) interacting with only one of the nanoantenna modes and transmits its energy to the nanoantenna through near-field interaction. The Hamiltonian of such a system has the form [20,35]:

$$\hat{H}_S=\hbar\omega_M\hat{a}^+\hat{a}+\frac{\hbar}{2}\omega_{TLS}\hat{\sigma}_z+\hbar\Omega_R\left(\hat{\sigma}^+\hat{a}+\hat{a}^+\hat{\sigma}\right), \tag{1}$$

where ω_{TLS} and ω_M are frequencies of the TLS transition and the antenna mode, respectively. The first term in Eq. (1) describes the nanoantenna mode; operators $\hat{a}^+$ and $\hat{a}$ are the creation and annihilation operators of a plasmon in the mode, and satisfy the commutation relation $\left[\hat{a},\hat{a}^+\right]=1$. The second term is the Hamiltonian of the TLS; $\hat{\sigma}^+$ and $\hat{\sigma}$ are transition operators from the ground, $|g\rangle$, to the excited, $|e\rangle$, states, and back, respectively; and $\hat{\sigma}_z=\left[\hat{\sigma}^+,\hat{\sigma}\right]$ is the population inversion operator of the TLS. The last term in Eq. (1)

Optics EXPRESS

describes the near-field interaction between the nanoantenna mode and the TLS in the Jaynes-Cummings form with the coupling constant $\Omega_R = -\mathbf{E}_M \cdot \mathbf{d}_{TLS} / \hbar$, where $\mathbf{d}_{TLS}$ is the matrix element of the dipole transition of the TLS and $\mathbf{E}_M$ is the electric near field per one plasmon, which is defined by the relation $\frac{1}{8\pi}\int dV \frac{\partial(\varepsilon'\omega)}{\partial\omega}|\mathbf{E}|^2 = \hbar\omega_M$ (for more detailed information about the second quantization procedure for the near field in dissipative dispersive media, see Refs [36–39].).

In the absence of the interaction between the nanoantenna and the dipole emitter, the eigenstates of the system consist of the nanoantenna and dipole emitter eigenstates, $|n,e\rangle$ and $|n,g\rangle$, where n is the number of quanta in the antenna's mode. Due to this interaction, the eigenstates of the system ($|m\rangle$, $\hat{H}_S|m\rangle = E_k|m\rangle$) are split dressed states, $|n,\pm\rangle$. These states are a superposition of the states in which the antenna mode has $n-1$ excited quanta and the TLS is in the excited state, $|e\rangle$, and where the mode has n quanta and the TLS is in the ground state, $|g\rangle$. They can be written in the form [20]:

$$|n,+\rangle = \cos\varphi_n |n-1,e\rangle + \sin\varphi_n |n,g\rangle,\ |n,-\rangle = -\sin\varphi_n |n-1,e\rangle + \cos\varphi_n |n,g\rangle, \quad (2)$$

$$E_{n,\pm} = \hbar(n+1/2)\omega_M \pm \hbar\sqrt{\Omega_R^2(n+1)+(\Delta/2)^2}, E_0 = -\frac{\hbar\omega_{TLS}}{2}, \quad (3)$$

where $\Delta = \omega_M - \omega_{TLS}$ and $\varphi_n = \tan^{-1}\left(2\Omega_R\sqrt{n+1}/\Delta\right)/2$. Thus, the interaction between the nanoantenna and the TLS results in the rearrangement of the eigenstates of non-interacting subsystems.

To describe the losses, we introduce three reservoirs interacting with the system. The Hamiltonian of these reservoirs has the form [19,40]:

$$\hat{H}_R = \hat{H}_R^{\text{rad}} + \hat{H}_R^{\text{deph}} + \hat{H}_R^{\text{J}} = \sum_{\mathbf{k},\lambda}\hbar\omega_k \hat{b}_{\mathbf{k},\lambda}^+ \hat{b}_{\mathbf{k},\lambda} + \sum_j \hbar\omega_j \hat{b}_j^+ \hat{b}_j + \sum_j \hbar\omega_j \hat{r}_j^+ \hat{r}_j \quad (4)$$

The first term describes the electromagnetic field of the free space, which is responsible for the radiative losses of the system. Operators $\hat{b}_{\mathbf{k},\lambda}^+$ and $\hat{b}_{\mathbf{k},\lambda}$ are creation and annihilation operators in the mode of the free electromagnetic field with wave vector $\mathbf{k}$, polarization λ, and frequency $\omega_{\mathbf{k}}$. The second term is a phonon bath which describes TLS dephasing, where $\hat{b}_j^+$ and $\hat{b}_j$ are the creation and annihilation operators of the phonon in the mode with frequency ω_j. The third term describes Joule losses in the metal of the plasmonic nanoantenna. The creation and annihilation operators $\hat{r}_j^+$ and $\hat{r}_j$ correspond to the excitation and relaxation of a phonon in the metal. These type of losses are nonradiative.

The Hamiltonian of the interaction of the system with the reservoirs can be written as:

$$\hat{H}_{SR} = \hbar\sum_{\mathbf{k},\lambda}\left[\kappa_{\mathbf{k},\lambda}^{\text{rad}}\hat{a}^+\hat{b}_{\mathbf{k},\lambda} + \kappa_{\mathbf{k},\lambda}^{\text{rad}*}\hat{a}\hat{b}_{\mathbf{k},\lambda}^+\right] + \hbar\sum_j \kappa_j^{\text{ph}}\hat{\sigma}_z\left(\hat{b}_j + \hat{b}_j^+\right) + \hbar\sum_j \kappa_j^{\text{nonrad}}\left(\hat{a}^+\hat{r}_j + \hat{a}\hat{r}_j^+\right). \quad (5)$$

The first term in Eq. (5) describes the interaction of modes of the free space and the plasmonic nanoantenna in the dipole approximation, $\hat{H}_{SR}^{\text{rad}} = -\mathbf{d}_M \cdot \mathbf{E}_{\text{free}}$, where $\hat{\mathbf{d}}_M = \mathbf{d}_M\left(\hat{a}+\hat{a}^+\right)$ is the dipole moment of the plasmonic mode of the nanoantenna with the

Optics EXPRESS

matrix element of the dipole moment $\mathbf{d}_M$, $\mathbf{E}_{\text{free}} = \sum_{\mathbf{k},\lambda} \sqrt{2\pi\hbar\omega_{\mathbf{k}}/V}\left(\mathbf{e}^{*}_{\mathbf{k},\lambda}\hat{b}^{+}_{\mathbf{k},\lambda}e^{-i\mathbf{kr}} + \mathbf{e}_{\mathbf{k},\lambda}\hat{b}_{\mathbf{k},\lambda}e^{i\mathbf{kr}}\right)$ is the electric field after the second quantization procedure, and $\kappa_{\mathbf{k},\lambda} = -\mathbf{d}_M \cdot \mathbf{E}_{\mathbf{k},\lambda}/\hbar$ is the coupling constant. The second term describes dephasing of the TLS, i.e. the process of emission and absorption of a quantum of the reservoir excitation in which the energy of the system does not change, but the average dipole moment (non-diagonal elements of its density matrix) decays [19,40]. The last term describes the interaction of phonons in the metal and the nanoantenna mode.

Using the Born-Markov approximation, and excluding reservoir variables, we obtain the master equation for the density matrix in the Lindblad form [19,41]:

$$\frac{\partial}{\partial t}\hat{\rho}_S(t) = -\frac{i}{\hbar}\left[\hat{H}_S, \hat{\rho}_S\right] + L\left[\hat{\rho}_S(t)\right], \tag{6}$$

where the Lindblad superoperator,

$$\begin{aligned} L\left[\hat{\rho}_S(t)\right] = &\sum_{mm'} \frac{\gamma_{\text{rad}}^{mm'} + \gamma_{\text{nonrad}}^{mm'}}{2}\left(2\hat{S}_a^{mm'}\hat{\rho}_S\left(\hat{S}_a^{mm'}\right)^{+} - \left(\hat{S}_a^{mm'}\right)^{+}\hat{S}_a^{mm'}\hat{\rho}_S - \hat{\rho}_S\left(\hat{S}_a^{mm'}\right)^{+}\hat{S}_a^{mm'}\right) \\ &+\sum_{mm'} \frac{\gamma_{\text{deph}}^{mm'}}{2}\left(2\hat{S}_{\sigma_z}^{mm'}\hat{\rho}_S\left(\hat{S}_{\sigma_z}^{mm'}\right)^{+} - \left(\hat{S}_{\sigma_z}^{mm'}\right)^{+}\hat{S}_{\sigma_z}^{mm'}\hat{\rho}_S - \hat{\rho}_S\left(\hat{S}_{\sigma_z}^{mm'}\right)^{+}\hat{S}_{\sigma_z}^{mm'}\right) \\ &+\sum_{mm'} \frac{\gamma_{\text{pump}}^{mm'}}{2}\left(2\left(\hat{S}_{\sigma}^{mm'}\right)^{+}\hat{\rho}_S\hat{S}_{\sigma}^{mm'} - \hat{S}_{\sigma}^{mm'}\left(\hat{S}_{\sigma}^{mm'}\right)^{+}\hat{\rho}_S - \hat{\rho}_S\hat{S}_{\sigma}^{mm'}\left(\hat{S}_{\sigma}^{mm'}\right)^{+}\right), \end{aligned} \tag{7}$$

describes the relaxation processes in the system due to interaction with reservoirs with rates γ_{rad}, γ_{nonrad}, γ_{deph}, and γ_{pump}. The operators $\hat{S}_a^{mm'} = \langle m|\hat{a}|m'\rangle|m\rangle\langle m'|$, $\hat{S}_{\sigma}^{mm'} = \langle m|\hat{\sigma}|m'\rangle|m\rangle\langle m'|$, and $\hat{S}_{\sigma_z}^{mm'} = \langle m|\hat{\sigma}_z|m'\rangle|m\rangle\langle m'|$ correspond to the transition of the system from eigenstate $|m\rangle$ to eigenstate $|m'\rangle$ of the system Hamiltonian $\hat{H}_S$ Eq. (2) due to the interaction of the system with the reservoirs [42]. The dimensionless coefficients $\gamma_{mm'}^{\text{rad}}$, $\gamma_{mm'}^{\text{nonrad}}$, and $\gamma_{mm'}^{\text{deph}}$ can be calculated using Fermi's golden rule. Assuming that the reservoirs are in thermal equilibrium, the Kubo-Martin-Schwinger condition holds for each of the transition rates, namely, $\gamma_{mm'}^{j}/\gamma_{m'm}^{j} = e^{-(E_m - E_{m'})/kT_i}$, where T_i is the temperature of the *i*-th reservoir. Note that in Eqs. (6) and (7), we add incoherent pumping of the TLS by introducing the term $\sim \gamma_{\text{pump}}$, which corresponds to the transition between the eigenlevels with increasing energy [43]. We assume that the temperature of the free space reservoir is zero, $T_{\text{rad}} = 0$, and the temperature of the pumping reservoir is $T_{\text{pump}} = -0$, so that interaction with this results in an energy transfer only from the reservoir to the system. The temperature of the reservoir of Joule losses can change. We investigate the dependence of the system behavior on this temperature. We suppose that the radiative and nonradiative losses of the nanoantenna and the TLS dephasing remain the same as for a non-interacting antenna and SPS. At the same time, the losses caused by the interaction of the TLS with the surrounding EM field in the vicinity of the nanoantenna are determined by the Rabi constant, Ω_R, and differ from the case of a free non-interacting TLS.

Since the off-diagonal elements of the density matrix $\hat{\rho}_S$ decay exponentially [44], we focus solely on the diagonal elements. Denoting these as p_m, and using Eqs. (6) and (7), we obtain [44]:

Optics EXPRESS

$$\dot{p}_m = \sum_{m'} \gamma_{mm'} p_{m'} - \left(\sum_{m'} \gamma_{m'm} \right) p_m \tag{8}$$

where

$$\gamma_{mm'} = \left(\gamma_{mm'}^{\text{rad}} + \gamma_{mm'}^{\text{nonrad}} \right) \left| \langle m | \hat{a} | m' \rangle \right|^2 + \gamma_{mm'}^{\text{deph}} \left| \langle m | \hat{\sigma}_z | m' \rangle \right|^2 + \gamma_{mm'}^{\text{pump}} \left| \langle m | \hat{\sigma}^+ | m' \rangle \right|^2 . \tag{9}$$

From the system of equations in (8), we can obtain the dynamics of the diagonal elements of the density matrix. We can then use these to calculate all the average values of the operators of interest at any moment in time, as $\left\langle \hat{A} \right\rangle = Tr(\rho(t)\hat{A}) = \sum_m p_m(t) \langle m | \hat{A} | m \rangle$. In the following, we consider the behavior of the second-order coherence function $g^{(2)}(0)$.

3. The plasmonic nanoantenna as a single-photon source

The second-order coherence function $g^{(2)}(0)$ can be written as [19,20]:

$$g^{(2)}(0) = \left\langle a^+ a^+ a a \right\rangle / \left\langle a^+ a \right\rangle^2 . \tag{10}$$

Here, we assume that the nanoantenna makes the main contribution to the radiation (which is much greater than that of the SPS). This assumption is reasonable because, as it has been mentioned in [18], when an atom or a molecule is coupled to the open resonator (e.g., nanoantenna) and high Purcell factors are achieved, the main part of the radiation to the modes of a free space comes from the open resonator while the main part of the atom energy transmits directly to the open resonator. Numerical simulations show that $g^{(2)}(0)$ depends strongly on the ratio $\hbar\Omega_R / kT$. From Fig. 1, we can see that at low pumping power $\gamma_{\text{pump}} << \gamma_{\text{nonrad}}$, $g^{(2)}(0)$ can take any values between 0 and 2 (the solid red curve). When the interaction is weak, $\hbar\Omega_R << kT$, and the pump power is low, $g^{(2)}(0) = 2$, which means that the nanoantenna radiates as a heat source. The function $g^{(2)}(0)$ decreases as the coupling increases; near $\hbar\Omega_R \sim kT$, $g^{(2)}(0)$ crosses over from 2 to 0. In the limit $\hbar\Omega_R >> kT$, $g^{(2)}(0)$ tends to 0, corresponding to the radiation of single photons. Thus, for a sufficiently strong interaction and a low pumping rate, the plasmonic nanoantenna emits single photons, in agreement with experiment [23,27,32].

It should be noted that an increase in the pumping rate, $\gamma_{\text{pump}} \sim \gamma_{\text{rad}}$, causes $g^{(2)}(0)$ to tend to unity, and the light from the system becomes coherent (see the dashed and dot-dashed curves in Fig. 1). This behavior corresponds to the coherent generation of the near-field in the nanoantenna; in this case, the system turns to a nanolaser. However, when only *one* SPS is used, this regime cannot be achieved, since the corresponding pumping rate is very high and cannot be obtained in experiments (see also Ref [45].). Thus, in the case of nanoantenna fed by *one* SPS, the real pumping rate is much lower than the threshold value. The case of zero pumping corresponds to the situation in which only the reservoir with a temperature greater than zero provides energy to the system. Note that at room temperature, in the optical region, the black body radiation is negligible and the system essentially does not radiate. To create radiation which can be detected, γ_{pump} should have a reasonable value that is greater than zero.

Thus, it is possible to observe single-photon emission from a nanoantenna by setting the required temperature and the pumping power of the TLS. The effect described here was obtained using a numerical simulation of Eq. (8). To clarify the mechanism of this effect, we consider a simplified model of the original problem.

Optics EXPRESS

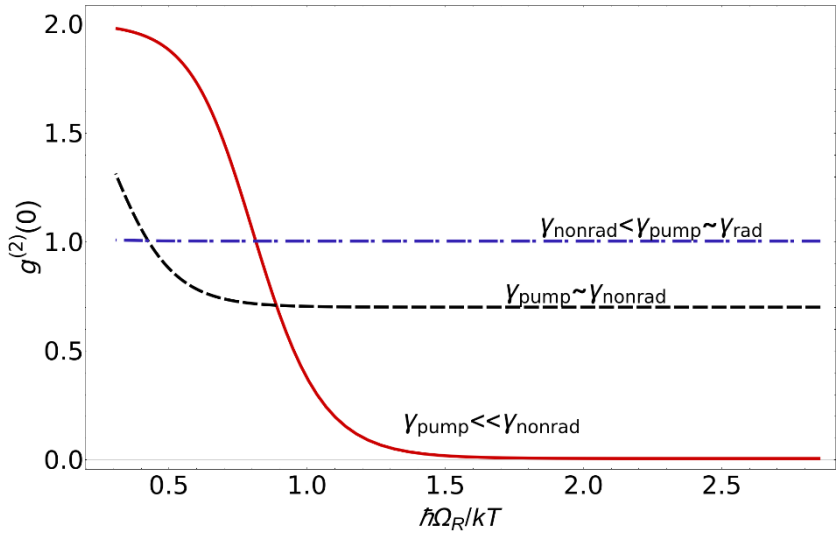

Fig. 1. $g^{(2)}(0)$ as a function of $\hbar\Omega_R / kT$ at different pumping rates. For the solid, dashed, and dot-dashed curves, the pumping rates are $\gamma_{\text{pump}} / \omega = 10^{-5}$, $\gamma_{\text{pump}} / \omega = 10^{-3}$, and $\gamma_{\text{pump}} / \omega = 0.05$, respectively. The parameters used in simulations are $\gamma_{\text{rad}} = 5 \cdot 10^{13}\,\text{s}^{-1}$, $\gamma_{\text{nonrad}} = 2 \cdot 10^{12}\,\text{s}^{-1}$, $\gamma_{\text{deph}} = 5 \cdot 10^{12}\,\text{s}^{-1}$, and $T = 300\text{K}$, corresponding to typical experimental values [27,32,45]. We assume here that the frequency of the nanoantenna mode and the frequency of optical transition in the SPS are the same, $\omega = \omega_M = \omega_{TLS} = 2.95 \cdot 10^{15}\,\text{s}^{-1}$. This frequency corresponds to a wavelength of $635\,\text{nm}$.

4. Low-quantum excitation limit

To understand the behavior described in the previous section, we consider a simplified model of the system consisting of a nanoantenna coupled to an SPS. Let us assume that the pumping power is zero and take into account only the excitations of the lower states, Eq. (2), which give first nonzero contributions to $g^{(2)}(0)$. These states are $|0,g\rangle$, $|1,+\rangle, |1,-\rangle$, and $|2,+\rangle, |2,-\rangle$, and their energy splits are:

$$\begin{aligned} \Delta_1 &= 2\sqrt{\Omega_R^2 + 1/4\left(\omega_M - \omega_{TLS}\right)^2} \\ \Delta_2 &= 2\sqrt{2\Omega_R^2 + 1/4\left(\omega_M - \omega_{TLS}\right)^2} \end{aligned} \tag{11}$$

Suppose for a moment that we have only the interaction with the reservoir of Joule losses, with temperature T. In this case, the system comes to thermal equilibrium with the reservoir, and the diagonal elements of the density matrix are then distributed according to Gibbs distribution [19], i.e.:

$$p_m \sim e^{-E_m/kT}. \tag{12}$$

where E_m is the energy of the m-th eigenstate. Using Eqs. (10) to (12), we can calculate $g^{(2)}(0)$:

$$g^{(2)}(0) = 2e^{-(2\Delta_1 - \Delta_2)/2kT} \frac{\left|\cos\varphi_2\right|^2 + e^{-\Delta_2/kT}\left|\sin\varphi_2\right|^2}{\left(\left|\cos\varphi_1\right|^2 + e^{-\Delta_1/kT}\left|\sin\varphi_1\right|^2\right)^2}. \tag{13}$$

Optics EXPRESS

Due to the factor $e^{-(2\Delta_1-\Delta_2)/2kT}$ in Eq. (13), $g^{(2)}(0)$ strongly depends on $(2\Delta_1-\Delta_2)/2kT$. In the particular case of resonance, when $\omega_M=\omega_{TLS}=\omega$, we have:

$$\Delta_1=2\Omega_R,\ \Delta_2=2\sqrt{2}\Omega_R. \tag{14}$$

Hence, in the limits $\hbar\Omega_R/kT>>1$ and $\hbar\Omega_R/kT<<1$ (Fig. 1, dashed and solid curves, respectively), at zero pumping rate, we obtain:

$$g^{(2)}(0)\sim 2,\ \hbar\Omega_R/kT<<1, \tag{15}$$

$$g^{(2)}(0)\sim \exp\left(-\left(2-\sqrt{2}\right)\hbar\Omega_R/kT\right)<<1,\ \hbar\Omega_R/kT>>1. \tag{16}$$

Expressions (15) and (16) are in qualitative agreement with the results of numerical simulation, as shown in Fig. 1. The obtained result can be qualitatively explained as follows. When the energy of thermal fluctuations, kT, is much higher than the interaction energy, $\hbar\Omega_R$, the occupation probabilities of the levels $|n,+\rangle$ and $|n,-\rangle$ are almost the same, and we effectively have equidistant levels $|n\rangle$ of a harmonic oscillator. In thermal equilibrium, the second-order coherence function for the harmonic oscillator is $g^{(2)}(0)=2$. When the energy of thermal fluctuations, kT, is much smaller than the interaction energy, $\hbar\Omega_R$, the occupation probability of the level $|n,-\rangle$ is much higher than that of $|n,+\rangle$, and we have a non-equidistant spectrum. In this case, $g^{(2)}(0)$ strongly depends on the distance between levels. At low temperature, for the energy levels given by Eq. (3) for the Jaynes-Cummings Hamiltonian (1), $g^{(2)}(0)=0$.

In the case of nonzero detuning, the results are qualitatively unchanged. When $\hbar\Omega_R/kT>>1$, $g^{(2)}(0)$ tends to zero. However, at a fixed ratio of $\hbar\Omega_R/kT$, when the frequency of the mode is higher than the frequency of the TLS, $g^{(2)}(0)$ becomes larger than in the case where the frequency of the mode is smaller than the frequency of the TLS. This follows from the fact that the first nonzero contribution to $g^{(2)}(0)$ originates from the state with two quanta of excitation in the plasmonic mode, i.e. with $n=2$. The eigenstate with the minimum energy for which $n=2$ is $|2,-\rangle=-\sin\varphi_2|1,e\rangle+\cos\varphi_2|2,g\rangle$, see Eq. (2), where the coefficients $\sin\varphi_2=\left(\left(\sqrt{3\Omega_R^2+(\Delta/2)^2}-\Delta/2\right)\Big/2\sqrt{3\Omega_R^2+(\Delta/2)^2}\right)^{1/2}$ and $\cos\varphi_2=\left(\left(\sqrt{3\Omega_R^2+(\Delta/2)^2}+\Delta/2\right)\Big/2\sqrt{3\Omega_R^2+(\Delta/2)^2}\right)^{1/2}$ depend on the detuning, Δ, and its sign. If $\Delta\to+\infty$, then $\sin\varphi_2\to 0$ and $\cos\varphi_2\to 1$, giving $|2,-\rangle\sim|2,g\rangle$, and this state gives a nonzero contribution to $g^{(2)}(0)$. In the opposite case, when $\Delta\to-\infty$, $\sin\varphi_2\to 1$ and $\cos\varphi_2\to 0$. The state $|2,-\rangle\sim-|1,e\rangle$ and this state does not contribute to $g^{(2)}(0)$. Thus, in the case of negative detuning, $g^{(2)}(0)$ becomes smaller than in the case of $\Delta>0$. These qualitative assumptions are confirmed by Eq. (15), which obtained directly from Eqs. (10) and (11).

$$g^{(2)}(0)=2\cdot\frac{p_{|2,+\rangle}\sin^2\varphi_2+p_{|2,-\rangle}\cos^2\varphi_2}{\left(p_{|1,-\rangle}\cos^2\varphi_1+p_{|1,+\rangle}\sin^2\varphi_1+p_{|2,-\rangle}(2\cos^2\varphi_2+\sin^2\varphi_2)+p_{|2,+\rangle}(2\sin^2\varphi_2+\cos^2\varphi_2)\right)^2}, \tag{17}$$

Optics EXPRESS

Figure 2 illustrates the behavior of the $g^{(2)}(0)$ function on the detuning Δ.

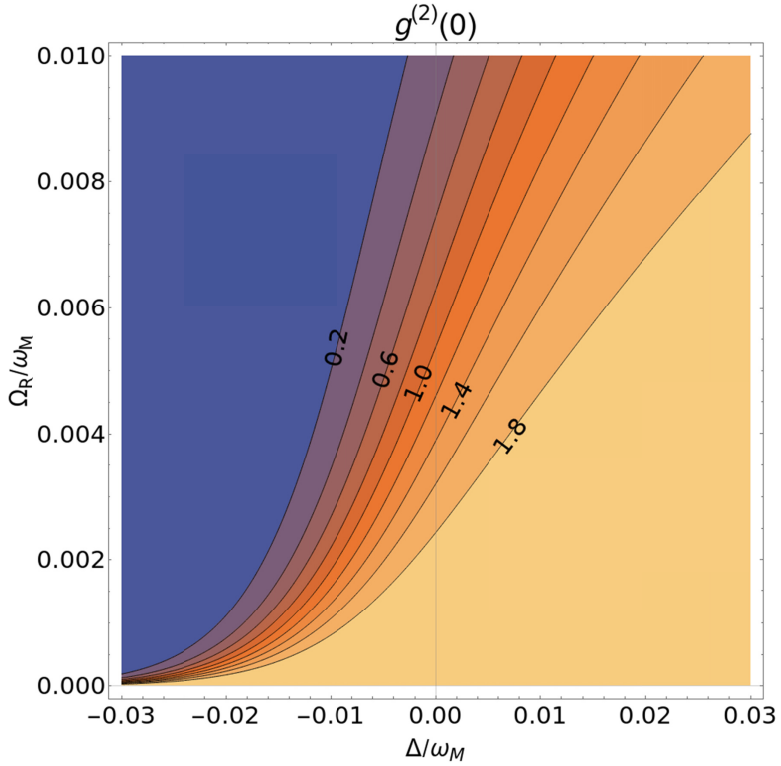

Fig. 2. The dependence of $g^{(2)}(0)$ on the detuning, Δ, and the interaction constant, Ω_R, obtained from Eq. (17).

5. Radiation intensity

As can be seen from Fig. 1, we can obtain $g^{(2)}(0)$ close to zero only in the limit of small pumping rates, which do not allow us to achieve a radiation intensity that is sufficient to exceed the intensity level of an individual SPS. Our goal is to find a value for the pumping power at which the nanoantenna emits rapidly but can still be considered an SPS, and can be useful in practical applications. We therefore need to find the maximum pumping rate at which the nanoantenna still has a coherence function $g^{(2)}(0)$ close to zero, and at the same time a radiation intensity that is sufficiently high. To describe this intensity, we calculate the rate of energy emission into the reservoir of radiation losses by the nanoantenna, $\langle \dot{H}_S \rangle_{\text{rad}} = \text{Tr}(L_{\text{rad}}(\rho)H_S)$. The dependence of $g^{(2)}(0)$ on $\langle \dot{H}_S \rangle_{\text{rad}}$ is a key characteristic of a plasmonic nanoantenna fed by an SPS. We demonstrate the possibility of overcoming the radiation intensity of an individual SPS and preserving single-photon properties for the plasmonic nanoantenna by using parameters close to ones from real experiments [27].

In sufficiently large limits of the pumping power of the SPS, the nanoantenna radiates as an SPS, and its radiation intensity is three orders of magnitude higher than that of a solitary SPS. The radiation intensity reaches one emission event per picosecond, i.e. the radiation rate increases up to THz (see Fig. 3).

Optics EXPRESS

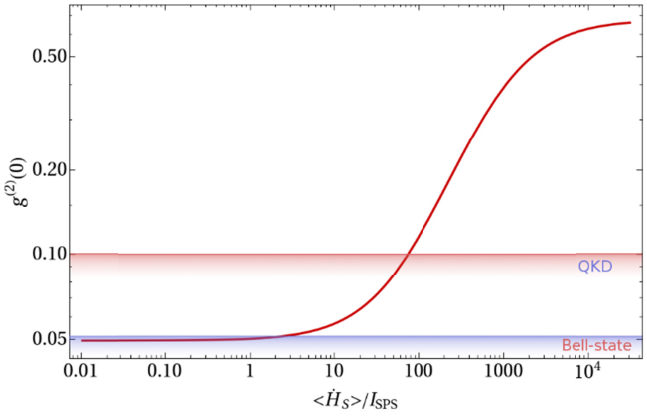

Fig. 3. The dependence of $g^{(2)}(0)$ on the radiation intensity of the nanoantenna divided by the intensity of a solitary SPS, $I_{SPS} = 10^9 \ \hbar\omega_{TLS}\ \mathrm{s}^{-1}$. The pump rate changes from $10^8\ \mathrm{s}^{-1}$ to $10^{12}\ \mathrm{s}^{-1}$; the rate of radiative and nonradiative losses are $\gamma_{\mathrm{rad}} = 5\cdot 10^{13}\ \mathrm{s}^{-1}$ and $\gamma_{\mathrm{nonrad}} = 2\cdot 10^{12}\ \mathrm{s}^{-1}$, respectively; and the the dephasing rate is $\gamma_{\mathrm{deph}} = 5\cdot 10^{12}\ \mathrm{s}^{-1}$. The zone below the red line displays the values required for the quantum key distribution (QKD) applications. The blue line indicates the values that are required for Bell-state sources.

6. Comparison to experiments

In recent experimental work [27], the authors used a CdSe/ZnS quantum dot as an SPS, which was coupled to a plasmonic nanoantenna (a silver cube lying on the quantum dot) at room temperature. If we suppose that the nanoantenna gives the main contribution to the radiation, then this system is similar to the one considered here. The quantum dot is located at the maximum of the electric field of the plasmonic mode of the antenna. The Purcell factor of the system is $F = 1900$, which corresponds to the Rabi constant of the interaction $\Omega_R \sim \sqrt{F\gamma_a\gamma_\sigma} \sim 5\cdot 10^{13}\ \mathrm{s}^{-1}$, and the detuning is $\Delta \sim 10^{13}\mathrm{s}^{-1}$. In the experiment in Ref [27], the value $g^{(2)}(0) = 0.32$ was obtained. Using the parameters from Ref [27]. in our model, and based on Eq. (8), and the qualitative Eq. (17), we obtain that $g^{(2)}(0) = 0.23$. Simulations of Eq. (8) show that $g^{(2)}(0)$ increases slightly with γ_{pump} at the same pumping rates that were used in the experiment, while the radiation intensity reaches $\sim 10^3$ times the intensity of a solitary SPS, corresponding to about 1 ps per radiation event. With a further increase in γ_{pump}, $g^{(2)}(0)$ tends to unity (see Fig. 1).

A setting similar to that described above was used in Ref [32]. The authors used an NV center as an SPS that was coupled to a plasmonic nanoantenna (a silver cube lying at the NV center). The Purcell factor of the system is about $F = 200$, which corresponds to a coupling constant of $\Omega_R \sim 10^{12}\ \mathrm{s}^{-1}$; the system is at room temperature and the difference between the frequency of the plasmonic mode and the NV center is zero. The system demonstrates a high rate of emission, $I = 56\cdot 10^6\ \mathrm{s}^{-1}$ at $\gamma_{\mathrm{pump}} \sim 10^{12}\ \mathrm{s}^{-1}$, which is 90 times faster than the rate of a solitary NV center. In this experiment, the second-order coherence function is $g^{(2)}(0) = 0.41$. The results of simulations of Eq. (8) and those obtained from the direct substitution of parameters into Eq. (15) are qualitatively similar, giving $g^{(2)}(0) = 0.6$. If the pump rate is further increased, the $g^{(2)}(0)$ function slowly increases to unity, as shown in Fig. 1.

Optics EXPRESS

In both cases, the radiation intensity $\left\langle \dot{H}_S \right\rangle_{\text{rad}}$ rates are larger than that for a single TLS, and may reach one radiation process per picosecond (for the parameters used in Refs [27]. and [32], the values are larger by two and three orders of magnitude, respectively). The quantitative distinction between the experimental results obtained in Refs [27]. and [32] (for the value of $g^{(2)}(0)$ and the radiation rates) is due to the significant difference in the Rabi constants of the systems and, consequently, the Purcell factors. Moreover, according to Fig. 3 and Eq. (17), a small negative detuning, $\omega_M < \omega_{TLS}$, can reduce the value of $g^{(2)}(0)$ even further, as observed in the experiment in Ref [27].

7. Conclusion

As discussed in the introduction, an attempt to increase the radiation rate of isolated SPSs by using plasmonic nanoantennas is expected to lead to the deterioration of single-photon radiation properties due to the contribution of nanoantenna (open-cavity) radiation to the total emission of the system. In the present paper, we demonstrate the possibility of a nanoantenna fed by an SPS radiating single photons at high rates. We show that the second-order coherence function of radiation, $g^{(2)}(0)$, depends strongly on the ratio between the energy of antenna thermal fluctuations, kT, and the interaction energy, $\hbar\Omega_R$, between the antenna near-field and the dipole moment of the SPS. When $\hbar\Omega_R << kT$, the system radiation is similar to the emission of a single plasmonic nanoantenna in a state of thermal equilibrium with $g^{(2)}(0)$ reaching a value of two. This result is intuitively understandable at high temperatures, as only the nanoantenna contributes to the radiation. However, when the interaction energy is large, $\hbar\Omega_R >> kT$, $g^{(2)}(0)$ is close to zero, which is characteristic of single-photon emission. This result follows from the fact that when the interaction is strong, the system spectrum is rearranged, i.e. the distance between split states increases and the population of these states deviates from the Gibbs distribution. This means that the nanoantenna ceases to radiate as a thermal source. It is shown here that for a sufficiently large pumping power of the SPS, the nanoantenna emission exhibits a single-photon nature, and that its radiation rate can be increased up to 10^{12} s^{-1} (see Fig. 3). The obtained result opens the possibility of creating a fast single-photon radiation source. This would allow for the use of SPSs based on a plasmonic nanoantenna in quantum cryptography applications [4]. For instance, nanoantenna radiation meets the QKD requirements [46], with $g^{(2)}(0) < 0.1$ (Fig. 3, red zone) and a repetition rate greater than 10^9 s^{-1}. Due to their small size and good on-chip integration, devices based on antenna-SPS systems may replace complicated and very large settings based on attenuated laser sources, which are currently widely used in QKD systems. In addition, the use of plasmonic nanoantennas as SPSs could find applications in areas such as boson sampling [47], photonic quantum walks [48] and perhaps in Bell-state sources [49] (see the blue zone in Fig. 3).

Funding

Foundation for the Advancement of Theoretical Physics and Mathematics “BASIS”; Russian Foundation for Basic Research (18-32-00596); Presidium of Russian Academy of Sciences (Program No. 7).

References

1. Quantum Cryptography Technology Experts Panel, “A Quantum Information Science and Technology Roadmap: Part 2: Quantum Technology,” (Advanced Research and Development Activity, 2004).
2. D. Bouwmeester, A. Ekert, and A. Zeilinger, *The Physics of Quantum Information* (Springer, 2000).
3. J. L. O’Brien, “Optical quantum computing,” Science **318**(5856), 1567–1570 (2007).

Optics EXPRESS

4. C. H. Bennett and G. Brassard, "Quantum cryptography: Public key distribution and coin tossing," Theor. Comput. Sci. **560**, 7–11 (2014).
5. J. L. O'Brien, A. Furusawa, and J. Vučković, "Photonic quantum technologies," Nat. Photonics **3**(12), 687–695 (2009).
6. S. Buckley, K. Rivoire, and J. Vučković, "Engineered quantum dot single-photon sources," Rep. Prog. Phys. **75**(12), 126503 (2012).
7. S. Strauf, N. G. Stoltz, M. T. Rakher, L. A. Coldren, P. M. Petroff, and D. Bouwmeester, "High-frequency single-photon source with polarization control," Nat. Photonics **1**(12), 704–708 (2007).
8. M. Steiner, A. Hartschuh, R. Korlacki, and A. J. Meixner, "Highly efficient, tunable single photon source based on single molecules," Appl. Phys. Lett. **90**(18), 183122 (2007).
9. T. Aoki, A. S. Parkins, D. J. Alton, C. A. Regal, B. Dayan, E. Ostby, K. J. Vahala, and H. J. Kimble, "Efficient Routing of Single Photons by One Atom and a Microtoroidal Cavity," Phys. Rev. Lett. **102**(8), 083601 (2009).
10. I. Aharonovich, S. Castelletto, D. Simpson, C. Su, A. Greentree, and S. Prawer, "Diamond-based single-photon emitters," Rep. Prog. Phys. **74**(7), 076501 (2011).
11. R. Albrecht, A. Bommer, C. Deutsch, J. Reichel, and C. Becher, "Coupling of a Single Nitrogen-Vacancy Center in Diamond to a Fiber-Based Microcavity," Phys. Rev. Lett. **110**(24), 243602 (2013).
12. A. Faraon, C. Santori, Z. Huang, V. M. Acosta, and R. G. Beausoleil, "Coupling of Nitrogen-Vacancy Centers to Photonic Crystal Cavities in Monocrystalline Diamond," Phys. Rev. Lett. **109**(3), 033604 (2012).
13. M. D. Eisaman, J. Fan, A. Migdall, and S. V. Polyakov, "Invited review article: Single-photon sources and detectors," Rev. Sci. Instrum. **82**(7), 071101 (2011).
14. E. M. Purcell, "Spontaneous emission probabilities at radio frequencies," Phys. Rev. Lett. **69**, 681 (1946).
15. A. Bennett, D. Unitt, P. Atkinson, D. Ritchie, and A. Shields, "High performance single photon sources from photolithographically defined pillar microcavities," Opt. Express **13**(1), 50–55 (2005).
16. A. Faraon, P. E. Barclay, C. Santori, K.-M. C. Fu, and R. G. Beausoleil, "Resonant enhancement of the zero-phonon emission from a colour centre in a diamond cavity," Nat. Photonics **5**(5), 301–305 (2011).
17. A. E. Krasnok, A. P. Slobozhanyuk, C. R. Simovski, S. A. Tretyakov, A. N. Poddubny, A. E. Miroshnichenko, Y. S. Kivshar, and P. A. Belov, "An antenna model for the Purcell effect," Sci. Rep. **5**(1), 12956 (2015).
18. S. I. Maslovski and C. R. Simovski, "Purcell factor and local intensity enhancement in surface-enhanced Raman scattering," Nanophotonics **8**, 429 (2018).
19. H. J. Carmichael, *Statistical Methods in Quantum Optics 1: Master Equations and Fokker-Planck Equations (Theoretical and Mathematical Physics)* (Springer, 2003).
20. M. O. Scully and M. S. Zubairy, *Quantum Optics* (Cambridge university Press, 1997).
21. P. Lombardi, A. P. Ovvyan, S. Pazzagli, G. Mazzamuto, G. Kewes, O. Neitzke, N. Gruhler, O. Benson, W. H. Pernice, and F. S. Cataliotti, "Photostable Molecules on Chip: Integrated Sources of Nonclassical Light," ACS Photonics **5**, 126–132 (2018).
22. A. V. Akimov, A. Mukherjee, C. L. Yu, D. E. Chang, A. S. Zibrov, P. R. Hemmer, H. Park, and M. D. Lukin, "Generation of single optical plasmons in metallic nanowires coupled to quantum dots," Nature **450**(7168), 402–406 (2007).
23. S. K. Andersen, S. Kumar, and S. I. Bozhevolnyi, "Coupling of nitrogen-vacancy centers in a nanodiamond to a silver nanocube," Opt. Mater. Express **6**(11), 3394–3406 (2016).
24. T. T. Tran, D. Wang, Z.-Q. Xu, A. Yang, M. Toth, T. W. Odom, and I. Aharonovich, "Deterministic coupling of quantum emitters in 2D materials to plasmonic nanocavity arrays," Nano Lett. **17**(4), 2634–2639 (2017).
25. H. Takata, H. Naiki, L. Wang, H. Fujiwara, K. Sasaki, N. Tamai, and S. Masuo, "Detailed Observation of Multiphoton Emission Enhancement from a Single Colloidal Quantum Dot Using a Silver-Coated AFM Tip," Nano Lett. **16**(9), 5770–5778 (2016).
26. R. Regmi, J. Berthelot, P. M. Winkler, M. Mivelle, J. Proust, F. Bedu, I. Ozerov, T. Begou, J. Lumeau, H. Rigneault, M. F. García-Parajó, S. Bidault, J. Wenger, and N. Bonod, "All-dielectric silicon nanogap antennas to enhance the fluorescence of single molecules," Nano Lett. **16**(8), 5143–5151 (2016).
27. T. B. Hoang, G. M. Akselrod, and M. H. Mikkelsen, "Ultrafast Room-Temperature Single Photon Emission from Quantum Dots Coupled to Plasmonic Nanocavities," Nano Lett. **16**(1), 270–275 (2016).
28. L. Schweickert, K. D. Jöns, K. D. Zeuner, S. F. Covre da Silva, H. Huang, T. Lettner, M. Reindl, J. Zichi, R. Trotta, A. Rastelli, and V. Zwiller, "On-demand generation of background-free single photons from a solid-state source," Appl. Phys. Lett. **112**(9), 093106 (2018).
29. K. Matsuzaki, S. Vassant, H.-W. Liu, A. Dutschke, B. Hoffmann, X. Chen, S. Christiansen, M. R. Buck, J. A. Hollingsworth, S. Götzinger, and V. Sandoghdar, "Strong plasmonic enhancement of biexciton emission: controlled coupling of a single quantum dot to a gold nanocone antenna," Sci. Rep. **7**(1), 42307 (2017).
30. H. Siampour, S. Kumar, and S. I. Bozhevolnyi, "Chip-integrated plasmonic cavity-enhanced single nitrogen-vacancy center emission," Nanoscale **9**(45), 17902–17908 (2017).
31. S. Dey, Y. Zhou, Y. Sun, J. A. Jenkins, D. Kriz, S. L. Suib, O. Chen, S. Zou, and J. Zhao, "Excitation wavelength dependent photon anti-bunching/bunching from single quantum dots near gold nanostructures," Nanoscale **10**(3), 1038–1046 (2018).
32. S. I. Bogdanov, M. Y. Shalaginov, A. S. Lagutchev, C.-C. Chiang, D. Shah, A. S. Baburin, I. A. Ryzhikov, I. A. Rodionov, A. V. Kildishev, A. Boltasseva, and V. M. Shalaev, "Ultrabright Room-Temperature Sub-Nanosecond Emission from Single Nitrogen-Vacancy Centers Coupled to Nanopatch Antennas," Nano Lett. **18**(8), 4837–4844 (2018).

Optics EXPRESS

33. B. Rousseaux, D. G. Baranov, M. Käll, T. Shegai, and G. Johansson, "Quantum description and emergence of nonlinearities in strongly coupled single-emitter nanoantenna systems," Phys. Rev. B **98**(4), 045435 (2018).
34. P. Zhang, I. Protsenko, V. Sandoghdar, and X.-W. Chen, "A Single-Emitter Gain Medium for Bright Coherent Radiation from a Plasmonic Nanoresonator," ACS Photonics **4**(11), 2738–2744 (2017).
35. L. Mandel and E. Wolf, *Optical Coherence and Quantum Optics* (Cambridge University Press, 1995).
36. V. Y. Shishkov, E. Andrianov, A. Pukhov, and A. Vinogradov, "Hermitian description of localized plasmons in dispersive dissipative subwavelength spherical nanostructures," Phys. Rev. B **94**(23), 235443 (2016).
37. B. Huttner and S. M. Barnett, "Quantization of the electromagnetic field in dielectrics," Phys. Rev. A **46**(7), 4306–4322 (1992).
38. W. Vogel and D.-G. Welsch, *Quantum Optics* (John Wiley & Sons, 2006).
39. E. Waks and D. Sridharan, "Cavity QED treatment of interactions between a metal nanoparticle and a dipole emitter," Phys. Rev. A **82**(4), 043845 (2010).
40. H.-P. Breuer and F. Petruccione, *The theory of Open Quantum Systems* (Oxford University Press on Demand, 2002).
41. E. B. Davies, "*Quantum Theory of Open Systems*," (Academic Press, 1976).
42. R. Kosloff, "Quantum thermodynamics: A dynamical viewpoint," Entropy (Basel) **15**(12), 2100–2128 (2013).
43. H. J. Carmichael, *Statistical Methods in Quantum Optics 2: Non-Classical Fields* (Springer Science & Business Media, 2009).
44. V. Y. Shishkov, E. S. Andrianov, A. A. Pukhov, A. P. Vinogradov, and A. A. Lisyansky, "Zeroth law of thermodynamics for thermalized open quantum systems having constants of motion," Phys. Rev. E **98**, 022132 (2018).
45. J. B. Khurgin, "How to deal with the loss in plasmonics and metamaterials," Nat. Nanotechnol. **10**(1), 2–6 (2015).
46. I. Aharonovich, D. Englund, and M. Toth, "Solid-state single-photon emitters," Nat. Photonics **10**(10), 631–641 (2016).
47. A. Aspuru-Guzik and P. Walther, "Photonic quantum simulators," Nat. Phys. **8**(4), 285–291 (2012).
48. M. Hillery, "Physics. Quantum walks through a waveguide maze," Science **329**(5998), 1477–1478 (2010).
49. S. Guha, H. Krovi, C. A. Fuchs, Z. Dutton, J. A. Slater, C. Simon, and W. Tittel, "Rate-loss analysis of an efficient quantum repeater architecture," Phys. Rev. A **92**(2), 022357 (2015).